TARGETS AND RETURN SIGNAL STRENGTH SESSION SUMMARY

Chair: Tom Murphy

This session consisted of five talks, three of which dealt with target design, testing, and analysis, and two of which dealt with absolute calibration of return signal strengths from laser ranging targets.

D. Arnold presented a summary of analytical results spanning a wide variety of topics, including: range corrections to LAGEOS and LARES; wavelength correction to LAGEOS for 850 and 425 nm light; Apollo lunar array diffraction patterns; hollow cube thermal analysis; retroreflector arrays for high-altitude satellites; diffraction patterns from and thermal analysis of Russian corner cubes; and range corrections associated with multi-photon returns to a single-photon avalanche detector (SPAD).

G. Delle Monache presented an overview of the Space Climatic Facility (SCF) in Frascati—a space/earth/sun simulation facility used to examine the thermal properties of retroreflector arrays in a space environment. The presentation included example thermal images of LAGEOS/LARES corner cubes under simulated space conditions, a description of the SCF's far-field diffraction pattern test capability, preliminary test results of the GPS3 array as part of the ETRUSCO experiment, and plans to test a LAGEOS mock-up in the near future. An invitation was extended to perform thermal tests of other retroreflector systems at the LNF facility.

V. Shargorodsky and V. Vasiliev described a new two-layer nested glass sphere retroreflector target, 17 cm in diameter, 7.5 kg in mass, with a 100,000 m^2 cross-section at 532 nm. The spherical target has been built, and is currently undergoing measurement tests of the return pattern in various conditions. The expected launch date is late 2007. Also presented was a concept possibility for a multi-layer retroreflective sphere that would work at two colors.

T. Murphy presented signal strength results from the APOLLO LLR station, comparing the highest return rates to date with a detailed link budget. Realistic diffraction patterns and de-rating factors were applied to the Apollo arrays. The result was a return signal strength substantially weaker than expected, by a factor of 15. Dust or surface abrasion are likely to blame.

J. Luck and C. Moore presented the results of a study to see if Optus-B or similar targets could be used to calibrate the return strength from other targets. By comparing return strengths from Optus-B and GPS on a variety of nights with similar pointing angles within a given comparison, they found that the measured cross-section ratio agreed with the theoretical ratio to better than 15%—suggesting such inter-comparisons as a viable technique for characterizing the performance of targets in the space environment.

Retroreflector Studies

David A. Arnold

1. 94 Pierce Road, Watertown, MA 02472, USA.

Contact: david-arnold@earthlink.net +1 617-924-3811.

Abstract

This paper discusses studies being done on retroreflectors. Complete reports are available for some, and others are ongoing projects. The studies include a preliminary transfer function for the LARES retroreflector array; computation of the wavelength correction for LAGEOS 850–425 nm; the cross-section of the Apollo lunar retroreflector arrays; parametric thermal analysis of a hollow beryllium retroreflector; retroreflector arrays for high-altitude satellites; measured diffraction patterns of retroreflectors; thermal simulations of coated and uncoated solid cube corners; and modelling of the response of a SPAD detector to various retroreflector arrays.

Introduction

This is an abbreviated version of the paper. The full paper in PDF format is available at http://www.ilrscanberraworkshop2006.com.au/workshop/day6/overview.asp or on the SPWG website in WORD format at http://nercslr.nmt.ac.uk/sig/signature.html.

LARES preliminary transfer function

The variations in range are reduced by the square root of the number of cube corners. Since LAGEOS has 4 times as many cubes as LARES the averaging is better by about a factor of 2. Because the radius of LARES is about half the size of LAGEOS the range correction is smaller. The two effects cancel each other approximately so the variation in the range correction is about the same for both satellites.

Wavelength correction for LAGEOS 850nm-425nm

Table 1 shows the wavelength correction (mm) vs velocity aberration (microradians). The average wavelength correction between 32 and 38 microradians is 2.806 ±.2 mm. The input polarization is circular.

***Table 1**: Range correction as a function of velocity aberration*

30	32	34	36	38	40
2.615000	2.773500	2.891750	2.865250	2.696250	2.465750

Cross section of the APOLLO Lunar retroreflector arrays

The APOLLO Lunar retroreflector arrays use a 1.5 inch diameter uncoated fused silica retroreflector with no intentional dihedral angle offset. The front face is recessed by half the diameter in a cavity with a 1.5 degree flare on the first APOLLO array and a 6 degree flare on the two later arrays. The cutoff angle with no flare would be 27.7 degrees. With the 1.5 degree flare it is 28.3 degrees. With the 6 degrees flare it is 30.3 degrees. Since the APOLLO retroreflectors are uncoated, there is loss of total internal reflection at certain incidence angles. The cross section has been computed vs incidence angle.

Parametric thermal analysis of hollow cubes

Equations have been derived for making order of magnitude estimates of the thermal gradients in a hollow Beryllium retroreflector due to absorption of solar radiation. The performance of the retroreflector can be degraded by thermal warping of the plates or changes in the dihedral angles between the reflecting plates as a result of differential expansion and contraction. The equations consider the case of conduction through the plate and along the plate.

Putting numbers into the equations shows that conduction through the plate is not a problem because the conduction path is wide and the path length short. Conduction along the plate can be a problem because the path length is long and the conduction path is narrow. Thermal distortion of the plates is acceptable as long as the cube corner is not larger than about 2 inches and the plate has a low solar absorptivity such as 7 percent.

Retroreflector arrays for high altitude satellites

Tables 2 and 3 show the area and mass of the cube corners needed to obtain a cross section of 100 million sq meters at the altitude of the GNSS satellites and a cross section of one billion sq meters at geosynchronous altitude.

***Table 2**: GNSS*

Design	# of cubes	Diam. in	Area sq cm	Mass g
uncoated	50	1.3	428	1000
coated	400	0.5	508	460
hollow	400	0.5	508	201
hollow	36	1.4	356	400
GPS	160	1.06	1008	1760

***Table 3**: Geosynchronous*

Design	# of cubes	Diam. In.	Area sq cm	Mass g
Uncoated	165	1.7	2415	7457
Coated	1153	.7	2863	3638
Hollow	1153	.7	2863	1590
Hollow	122	1.8	2003	2863
Single dihedral	22	2.0	446	708

Measurements of Russian cube corners

The data used in this analysis were kindly provided by Vladimir Vasiliev. A measurement of a reference mirror the same size as the cube corner is used for absolute calibration of the cross section of the cube corner. The first cube corner is a very high quality diffraction limited cube and the second is a typical cube corner. The cross section of the typical cube is larger than that of a diffraction limited cube corner past about 20 microradians.

Thermal simulations of Russian cube corner

These simulations were done using a very simple thermal simulation program that has been used only to give order of magnitude effects. The cube corners have no intentional beam spread. The isothermal diffraction does not show sufficient cross section at 26 microradians to account for the nominal cross section of the GPS array. The simulations with solar illumination show that thermal gradients could spread the

beam sufficiently to increase the cross section of the GPS array to 20 million sq meters that is the nominal cross section. The simulations show that the thermal gradients disappear quickly when the solar illumination stops. This could make it difficult to study the effect of thermal gradients in the laboratory. In the absence of a detailed engineering data on the cube corners the only way to know how the Russian cube corners behave is by laboratory testing.

Laboratory tests of cube corners

The space climactic facility at LNF in Frascati, Italy presently has a section of the LAGEOS retroreflector array, a section of LARES cube corners, and the third GPS array that contains Russian cube corners. The plan is to take diffraction patterns similar to those described in section 7 of this report and do thermal vacuum tests to measure the response of the cube corners to solar radiation. These test results can be compared to the simulations given in section 8 of this report. There will probably be significant differences between the simulations and the laboratory tests because of the limitations in the modelling.

Modelling of the response of a SPAD detector to a distributed signal

My analysis programs compute the range correction of a retroreflector array for centroid and constant fraction discriminator detection systems. All single photoelectron systems measure the centroid. For multi-photoelectron signals the range correction for a SPAD detector requires modelling the current vs time as a function of the time of arrival of each photoelectron. The exponential model of a SPAD assumes the number of charge carriers increases exponentially after a photon is detected until the available charge carriers are depleted. Tom Murphy has suggested modelling the number of charger carriers as a quadratic function of time on the assumption that the region of charge carriers is a thin disc whose radius increases linearly with time. The actual behaviour is complex. The rise time of a SPAD detector is a function of the number of photoelectrons. The CSPAD detector compensates for the number of photoelectrons for a point reflector. In the exponential model the rise time is independent of the number of photoelectrons. The exponential model does not explain the observed dependence of the rise time on the number of photoelectrons.

Simulations with the exponential model indicate that the measured range decreases if additional photoelectrons arrive before the current from the first photoelectron has increased to a large value.

***Table 4**: Two-photon bias*

x	0.0	2..6	5.2	10.4	15.6	20.8	26.0	52.0
Δr	3.60	2.66	1.77	0.72	0.28	0.10	0.04	0.00

In Table 4, 'x' is the one-way distance between the reflection points of two photoelectrons. Δr is the decrease in the measured one-way range due to the second photoelectron. For millimeter accuracy ranging the effect is significant for the first centimeter.

The modelling of a SPAD is complex. Unless one has a good model the only way to study the effect of a photoelectron that arrives a short time after the first is to do an experiment. For example, the target calibration vs signal strength could be done with a flat target and with a target where half the area is at position zero and the other half is a few millimeters farther away.

The INFN-LNF Space Climatic Facility for LARES and ETRUSCO

D. Arnold[1], G. Bellettini[2], A. Cantone[3], I. Ciufolini[4], D. G. Currie[5], S. Dell'Agnello[3], G. O. Delle Monache[3], M. Franceschi[3], M. Garattini[3], N. Intaglietta[3], A. Lucantoni[6], T. Napolitano[3], A. Paolozzi[6], E. C. Pavlis[7], R. Tauraso[2] and R. Vittori[8]

1. NASA-GSFC.
2. Univ. of Rome Tor Vergata, Italy.
3. INFN – LNF, Laboratori Nazionali di Frascati, Italy.
4. Univ. of Lecce, Italy.
5. Univ. of Maryland, College Park, USA.
6. Univ. of Rome La Sapienza, Italy.
7. Univ. of Maryland, Baltimore, USA.
8. Italian Air Force.

Abstract

The construction of the LNF Space Climatic Facility (SCF) started in Frascati, Italy, in 2006. The initial purpose was to study the thermal thrusts (TTs) of LAGEOS I/II satellites and to perform the full space-climatic and laser-optical characterization of the new LARES laser-ranged test mass. In late 2004 the construction of LARES was proposed to INFN, which then gave the scientific approval of the LARES experiment in November 2006.

The modular and evolutionary design of the SCF turned out to be well suited to characterize the thermal and optical performance of retro-reflector CCR arrays deployed on GNSS constellations. For this purpose, the groups of INFN-LNF, Rome-Tor Vergata plus R. Vittori in 2006 proposed to INFN a new experiment, ETRUSCO ("Extra Terrestrial Ranging to Unified Satellite COnstellations"). ETRUSCO was approved by INFN in October 2006. This paper describes the SCF and the first preliminary measurements and thermal simulations.

The SCF Apparatus

A schematic view of the SCF is shown in Fig. 1. The steel cryostat is approximately 2 m length by 1 m diameter. Inside this vacuum shell the shield, black painted with the high emissivity paint Aeroglaze® 306, is cooled down to 77 K by forced LNF2 flow. When the SCF is cold, the vacuum is typically 10^{-6} - 10^{-5} mbar.

The thermal input loads are provided by a Solar Simulator (SS) and an infrared (IR) Earth Simulator (ES). The SS is located outside, behind a quartz window (36 cm diameter, 4 cm thickness), which is transparent to the solar radiation up to 3000 nm. The ES located inside, is an Al black-painted disk (diam. 300 mm) held at 254 K by thermo coolers (TECs). A support fixture on the ceiling holds the prototype in front of the simulators. The distance of prototype from the ES is such to provide the CCRs with the same viewing angle in orbit (~60^{o} for LAGEOS). A Germanium window on the right side of the SCF allows for the acquisition of thermograms of the prototypes with an IR digital camera.

The SS (www.ts-space.co.uk) gives a 40 cm diameter beam with close spectral match to the AM0 standard of 1 Sun in space (1366.1 W/m^2), with a uniformity better than ± 5% over an area of 35 cm diameter. The spectrum is formed from the output of two sources, namely an HMI arc lamp (UV-V), together with a tungsten filament lamp (Red-IR). The quartz halogen lamp (with the tungsten filament) has a power of 12 KW, while the metal halide lamp has 6 KW power. These two sources are filtered

such that when the two beams are combined with a beam splitter/filter mirror, the resulting spectrum is a good match to AM0 in the range 400–1800 nm. The spectrum has also been measured also from λ = 1500 nm up to 3000 nm and found to be in reasonable agreement with the AM0 over this extended range. The absolute scale of the SS intensity is established by exposing the beam to a reference device, the *solarimeter*, which is a standard www.epply.com thermopile.

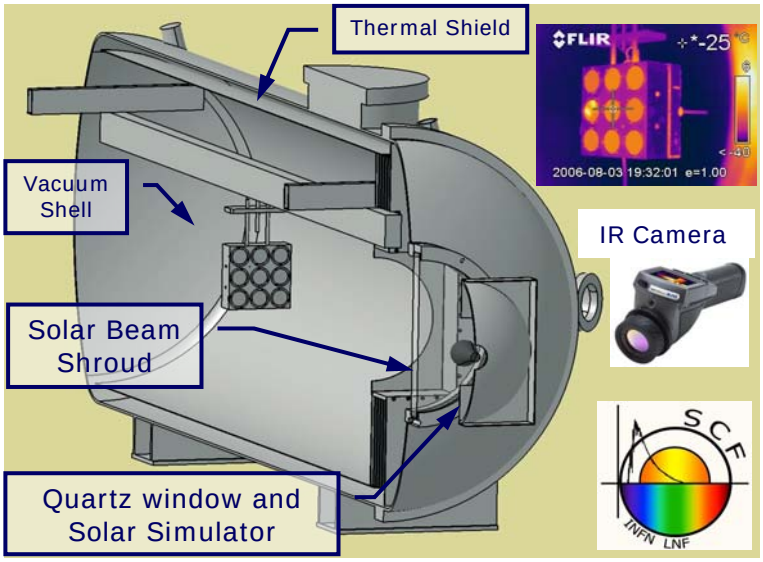

***Figure 1**: The LNF Space Climatic Facility with a retro-reflector array inside.*

The temperature DAQ system consists of an IR camera for non-invasive, high spatial granularity measurements and class-A PT100 RTDs with 4-wire readout. The IR camera is a ThermaCAM® EX320 by http://www.flir.com. The camera focal plane array detector is an un-cooled Vanadium Oxide micro-bolometer with spectral range 7.5 ÷ 13 μm. This camera has a true, built-in 320 x 240 pixel array, field of view/min focus distance 25° x 19° / 0.3 m and thermal sensitivity 80 mK. Since the EX320 factory accuracy is 2 K, the PT100s will be used for cross calibration. The PT100s are certified to have an accuracy of 0.1 – 0.3 K between 273 K and 373 K, which has been checked with a reference thermometer of absolute scale accuracy < 0.1 K, in a range appropriate for LAGEOS. The PT100s are also used below 250 K, outside the working range of the IR camera.

***Figure 2**: The 3×3 LAGEOS matrix built at LNF and the CCR assembly components.*

Thermal Characterization of LAGEOS Retro-reflectors

The thermal relaxation time of LAGEOS and LARES CCRs, τ_{CCR}, has never been measured in realistic climatic conditions. Computations vary by 300%. The goal for LARES and LAGEOS is to measure τ_{CCR} at ≤10% accuracy. This will make the error on the measurement of the Lense-Thirring effect due to thermal perturbations

negligible (permil level; [1] and references therein). A prototype called "3×3 matrix" has been built by LNF to measure directly τ_{CCR} and the time relaxation constant of the retainer Al rings (see fig. 2).

The program of measurements to be done on LAGEOS prototypes is described in [1] and will not be repeated here. The Aluminium base of this prototype has been held at constant temperature by the TECs (for example T(Al) = 298 K), in order to simulate the average temperature of LAGEOS, while the CCR assembly components experience the SS and ES thermal loads in varying climatic configuration. Note that the baseline LARES design uses the same type of LAGEOS CCRs.

The SCF includes thermal software for simulation and parametric design of spacecrafts and/or components. LNF is using the following package from http://www.crtech.com/: Thermal Desktop, the CAD-based geometric thermal modeler, RadCad, the radiation analysis module and orbital simulator, Sinda-Fluint, the solver. With this software, we estimated the overall TTs on LAGEOS during the eclipse due to the Earth shadow (see ref. [1]). With the SCF a preliminary thermal measurement with the ES as the only thermal input has been performed. The measured steady-state temperature of the CCR shows a fair match with the simulated thermal model of the 3×3 matrix (see fig. 3). It should be pointed out, however, that this preliminary test has been carried out with a non-optimized configuration of the screws and retainer rings (in terms of the materials used and of the torque applied to the screws) and that the temperature scale of IR camera was not fully calibrated. Once the thermal model will have been tuned to the final data it can be used for the complete thermal analysis of the LAGEOS satellites (and for the parametric design of LARES).

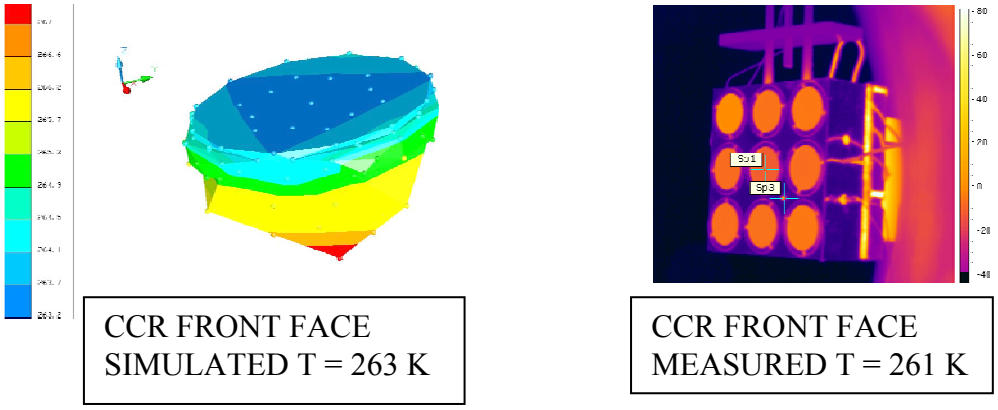

***Figure 3**: Comparison of the steady state CCR temperature measured with the SCF (ES only) and modelled with the thermal software, in a specific test configuration.*

Figure 4 shows the result of another preliminary in-air test at STP conditions, which was performed with the SS as main thermal load (at 75% of the nominal intensity). This was done mainly to exercise the whole system during a maintenance period of the SCF.

The SCF is now being upgraded with one optical-quality fused silica window to measure the far field diffraction patterns (FFDPs) of CCRs inside the SCF in realistic space conditions. Integrated thermal and optical tests will be performed on the CCRs of the LAGEOS "sector" prototype of NASA-GSFC (fig. 5). The finish of its Al surface is believed to be highly emissive (20% - and it will be measured) like for LAGEOS I. The sector contains 37 CCRs of good optical quality (in terms of the

accuracy of the dihedral angle offsets) with an outer diameter of 34 cm, well within the diameter of the SS beam.

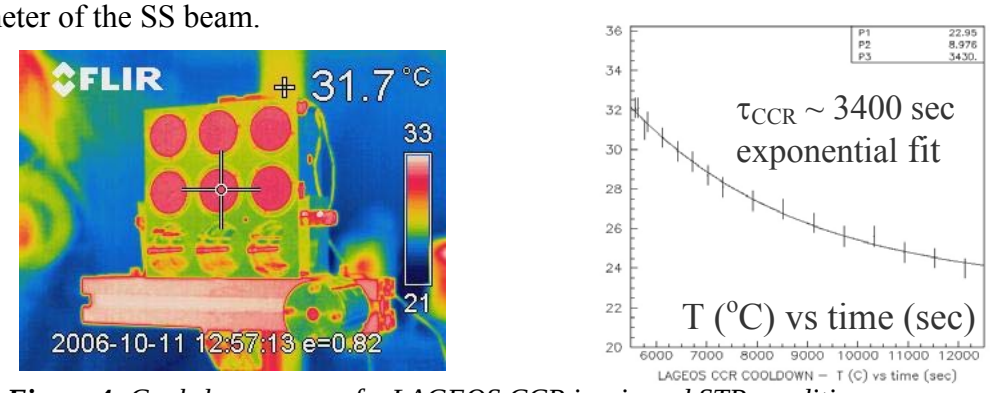

***Figure 4**: Cool-down curve of a LAGEOS CCR in-air and STP conditions.*

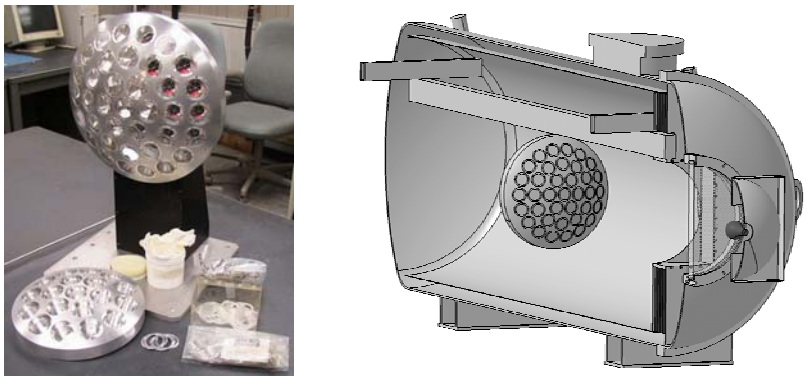

***Figure 5**: Engineering model of LAGEOS (circa 1992) property of NASA-GSFC. This LAGEOS sector is now at LNF for thermal and optical testing at the SCF.*

ETRUSCO (ExtraTerrestrial Ranging to Unified Satellite COnstellations)

The "unification" refers to the addition of laser ranging to the standard microwave ranging of GNSS satellites. Our aim is to perform a complete thermal and laser optical characterization of different CCR arrays used for existing and future GNSS constellations.

A preliminary in-air and STP test of a flight model of the third CCR array to be deployed on a satellite of the GPS block II has been done at LNF. This so-called "GPS3" array is identical to the ones installed on the GPS 35 and 36 satellites in orbit and is property of the University of Maryland (C. O. Alley et al). The three arrays have been manufactured in Russia. Mechanical drawings for its correct modelling have been provided courtesy of V. Vassiliev of the IPIE, Moscow. The GPS3 is currently at LNF, under a special agreement between NASA-GSFC, UMD and INFN-LNF. to be tested at the SCF. A preliminary test was done with the SS as main thermal load (at 75% of the nominal intensity). Two thermograms are shown in Fig. 6.

Figure 7 shows the thermal behaviour of the GPS3 as measured with the IR camera. A space-climatic test will follow in 2007, under the supervision of D. G. Currie of UMD.

Far Field Diffraction Pattern Measurement

The optical circuit for FFPD measurements at STP conditions is shown in fig. 8. The laser beam profiler is a Spiricon CCD camera. Tests are now performed at STP; final one will be performed with the CCR array in SCF.

Figure 9 shows how the SCF is now being upgraded with one optical-quality fused silica window to measure the far field diffraction patterns (FFDPs) of CCRs inside the SCF.

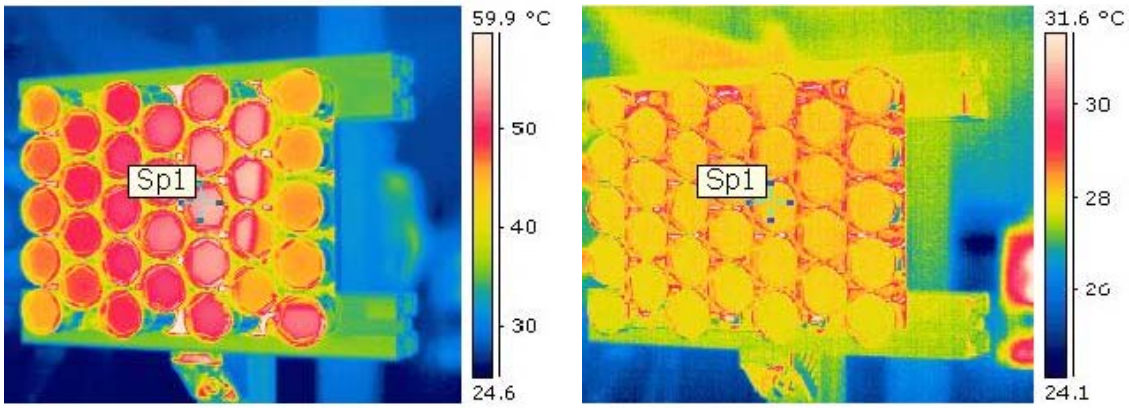

***Figure 6**: Warmest and coolest conditions of the GPS3 retro-reflectors in the LNF STP test.*

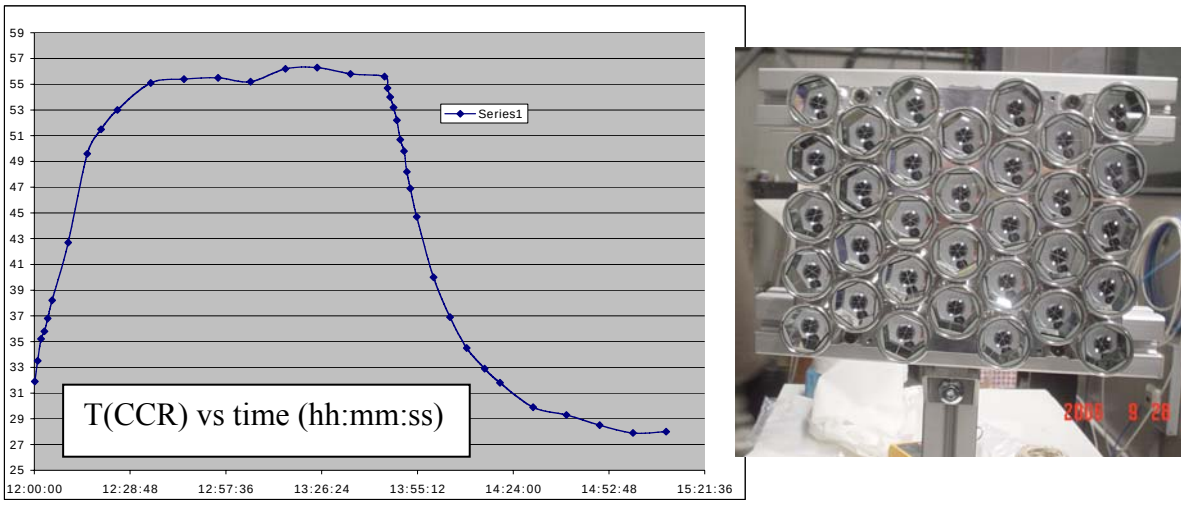

***Figure 7**: Warm-up and cool-down curves of the GPS3, in-ar and at STP at LNF.*

Each CCR will be first exposed to the Sun and the Earth simulators and its thermogram taken by the IR camera from the 45° window. Then, the CCR will be moved in front of the optical window to be exposed to the laser beam and its FFPD recorded (see fig. 10).

Conclusions

At the end of 2006 the SCF has become a permanent, small-size, experimental apparatus of INFN-LNF. The collaboration with ILRS has been very fruitful. Two approved INFN experiments are based for a significant part on the SCF operation: the by-now consolidated LARES mission and the new ETRUSCO experiment. The current upgrade of the SCF, consisting of the integration of the thermal and the laser-optical tests has been funded by INFN, and by LNF, explicitly for ETRUSCO. This funding includes an additional, dedicated optical table to be installed next to the SCF. It does not include the mechanical system(s) for the automated positioning of all the CCRs in the SCF climatic conditions. An endorsement of this work and its scientific motivations by ILRS would be very useful for fund-raising (outside ILRS) and the fulfilment of the ultimate ETRUSCO goals.

References

[1] *Probing Gravity in NEO with High-Accuracy Laser-Ranged Test Masses*, A. Bosco et al, Report INFN-LNF-06-24(P): http://www.lnf.infn.it/sis/preprint/pdf/LNF-06-24(P).pdf. Presented by S. Dell'Agnello at the "Quantum to Cosmos" NASA Int. Workshop, Warrenton (VA), USA, May 2006; to be published in a special issue of Int. Jour. Mod. Phys. D.

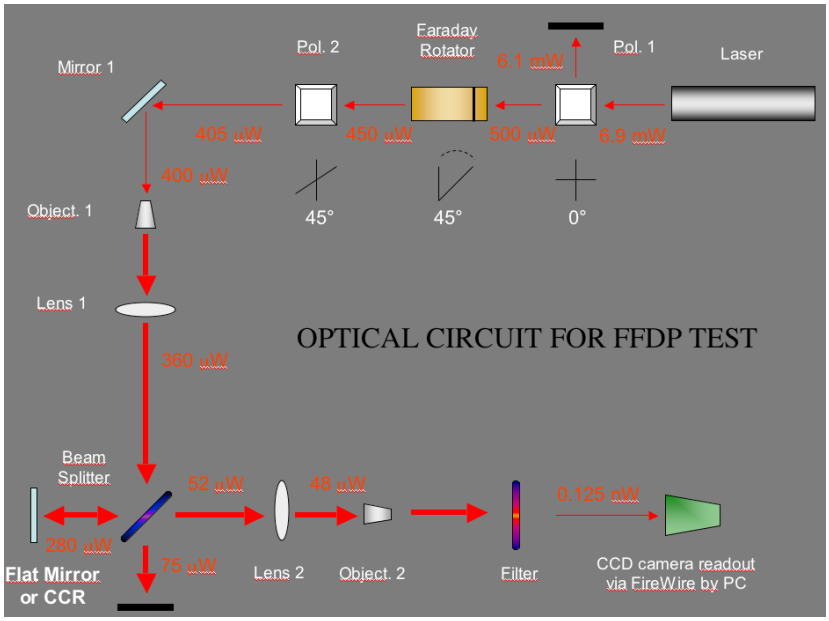

***Figure 8**: Layout of the optical circuit for the FFDP measurement.*

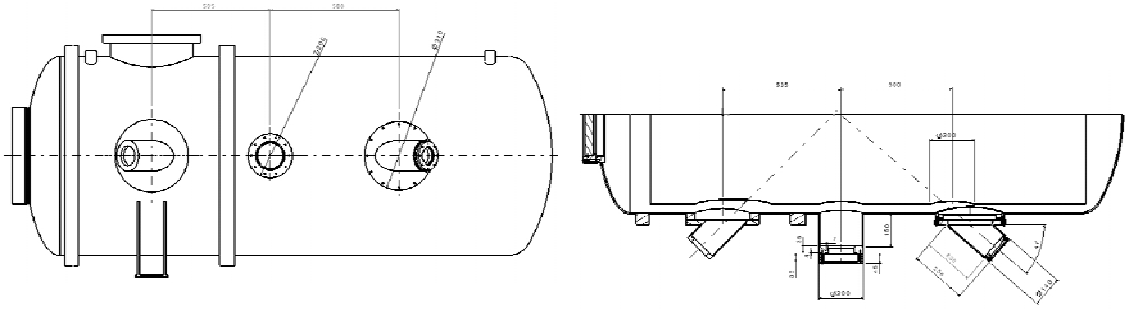

***Figure 9**: Left/central/right windows: IR thermometry, FFDPs and a spare.*

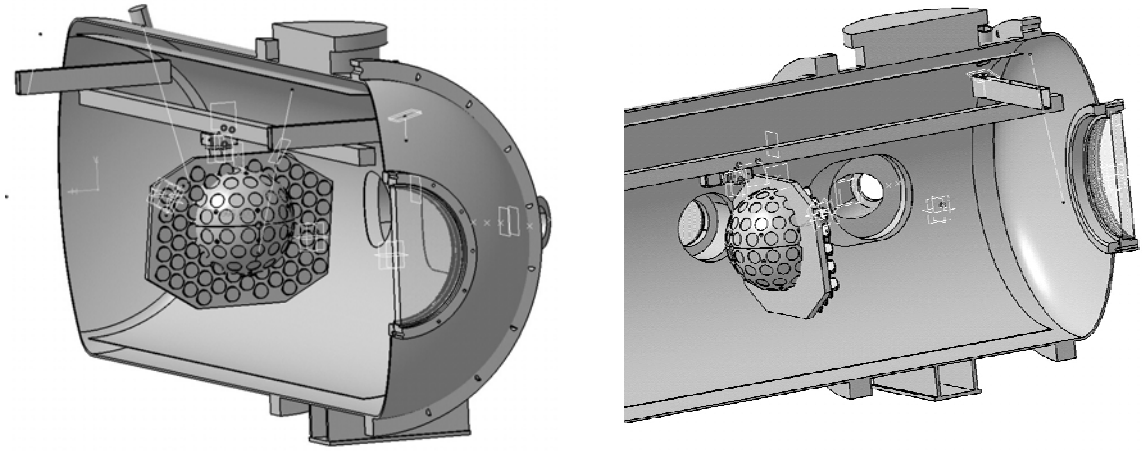

***Figure 10**: The baseline LARES and a GNSS retro-reflector array in the upgraded SCF.*

Absolute Calibration of LLR Signal: Reflector Health Status

T. W. Murphy, Jr. [1], E. G. Adelberger[2], J. B. Battat[3], C. D. Hoyle[4], E. L. Michelsen[1], C. W. Stubbs[3], and H. E. Swanson[2]

1. UC San Diego, MC-0424, 9500 Gilman Drive, La Jolla, CA 92093-0424, USA;
2. University of Washington, MC-351560, Seattle, WA 98195-1560, USA;
3. Harvard University, Dept. of Physics, 17 Oxford Street, Cambridge, MA 02138, USA;
4. Humboldt State University, Dept. of Physics, Arcata, CA 95521, USA;

Abstract

The recently-operational APOLLO lunar ranging station has received lunar return signals as strong as 0.6 photons per pulse over short periods. This signal rate is high enough to allow system optimization and diagnoses that permit careful quantification of system performance. Moreover, observing a spatially flat part of the moon with a well-defined field of view yields a check on the total one-way system efficiency. We are therefore able to compare the lunar signal rate against theoretical expectations as a means of examining the health of the retroreflector arrays after 35 years or more in space. A key part of this analysis is a thorough understanding of the diffraction pattern returned by the corner cube array.

Introduction

Three of the Apollo lunar landing missions placed corner-cube arrays on the lunar surface for the purpose of laser range measurements. The arrays consist of identical 38 mm-diameter uncoated fused-silica corner cubes working via total internal reflection. The Apollo 15 array is three times larger than the first two (Apollo 11 and Apollo 14), making it the preferred target due to its higher return rate. Roughly 85% of laser range measurements to the moon utilize the Apollo 15 array. The present analysis concerns itself only with this array, though results from the others support our conclusions.

The photon count per pulse can be characterized by the link equation,

$$N_{\rm detect} = N_{\rm launch}\eta_{\rm c}^2\eta_{\rm r}\eta_{\rm NB}Qn_{\rm refl}\eta_{\rm refl}\left(\frac{d}{r\phi}\right)^2\left(\frac{D_{\rm eff}}{r\Phi}\right)^2, \qquad (1)$$

where $N_{\rm launch}$ is the number of photons emitted by the laser per pulse, $\eta_{\rm c}$ is the one-way optical efficiency common to both transmit and receive modes, $\eta_{\rm r}$ is the optical efficiency of the receiver, $\eta_{\rm NB}$ is the narrow-band filter peak transmission, and Q is the detector quantum efficiency. The reflector array is composed of $n_{\rm refl}$ corner cubes (300 for Apollo 15), each of diameter, d and efficiency $\eta_{\rm refl}$. The uplink beam has a divergence ϕ, while the downlink divergence is Φ. $D_{\rm ef}$ is the effective diameter of the telescope (such that the collecting area is $\pi D_{\rm eff}^2/4$, and r is the one-way distance between the telescope and the reflector array. The simplified link equation assumes "tophat" diffraction distributions rather than Gaussian or more complicated patterns as a rough estimate of flux in the center of the distribution. We will later abandon this simplification in a refined approach.

The sections below evaluate the terms in the link equation for the recently constructed APOLLO (Apache Point Observatory Lunar Laser-ranging Operation) apparatus [1], comparing the model to observed peak rates. First, the individual terms and their

errors are estimated, followed by a check of the one-way efficiency using the solar-illuminated lunar surface. Then the lunar return is estimated and compared to actual measurements. Ultimately, the calculation is modified to account for a realistic diffraction pattern from the lunar corner cubes. An attempt is made to propagate realistic errors throughout this analysis.

One-Way Throughput

The one-way throughput of the apparatus may be checked by looking at a star or other flux standard using the same detector path employed in detecting lunar laser returns. This checks the quantity $\eta_c \eta_r Q$ in the link equation.

The η_c and η_r terms are composed of a number of optical efficiencies, evaluating to 0.51±0.03 and 0.29–0.58, respectively. Atmospheric transmission, measured to be 0.87 for one airmass at 550 nm at Apache Point, is included in η_c. The large range on η_r stems from the fact that the APOLLO detector only spans 1.4 arcseconds on a side. Therefore, a point source above the atmosphere may overfill the array depending on atmospheric seeing. Despite the large range, given knowledge of the seeing we can estimate this parameter to ~10% precision, leading to a ~12% estimate on η_r. The detector quantum efficiency, *Q*, is roughly 0.30. This number matches theoretical expectations based on device structure, and the flux calibration to a flux standard is in agreement with this figure. The effective diameter of the Apache Point 3.5 meter telescope is 3.26 m.

For the purpose of estimating the one-way throughput when looking at a flux standard, we need to know that the effective bandpass of the narrow-band filter is $\Delta\lambda_{NB}$ = 0.95 nm, and that the integration time is Δt_{APD} = 95 ns per APD gate event. We use the flux calibration standard that a zero-magnitude source at 532 nm wavelength has a flux density of $F_0 = 3.9\times10^{-11}$ W m^{-2} nm^{-1}. The number of photons we see per gate event is then

$$N = \frac{\pi}{4h\nu} F_0 10^{-0.4m} D^2 \Delta\lambda_{NB} \Delta t_{APD} \eta_c \eta_r Q \,, \qquad (2)$$

where *m* is the stellar magnitude, and $h\nu$ is the photon energy. During full moon, we estimate the darker-than-average terrain around the Apollo 15 reflector to have a surface brightness of 3.60 magnitudes per square arcsecond. This translates to 2.87 magnitudes into the 1.4×1.4 arcsecond field of view. Accounting for the fact that only 13 of the 16 APD elements are operational, the expected lunar background rate is: $N_{lunar} = 0.40 \pm 0.08$ photons per gate. Comparing this to the measured full-moon background rate of 0.40 photons per gate, we claim to understand the one-way efficiency of our system. Similar analysis on a focused star yields similar results.

Lunar Return Rate

Simplified Calculation

Populating the terms in Equation (1), we take $\eta_{NB} = 0.35 \pm 0.025$, $N_{launch} = f_{launch} E_{pulse} / h\nu$, with $f_{launch} = 0.6 \pm 0.03$ as the geometrical loss of the Gaussian beam propagating out of the 3.5 meter telescope, and $E_{pulse} = 0.100$ J. Setting $n_{refl} = 300$, d = 0.038 m, $\eta_{refl} = 0.93$, $r = 3.85\times10^8$ m, $\phi = 0.8 \pm 0.12$ arcseconds, and $\Phi = 10 \pm 1.5$ arcseconds, we get an expected lunar return into the APD array (with its particular pattern of dead pixels) of: $N_{detect} = 12.0 \pm 6.1$ photons per pulse. If we use the information we get from the one-way system check, we

reduce the uncertainty by a small amount to ±5.6 photons per pulse.

Observed Lunar Return Rate

The APOLLO lunar return rate is highly dependent on atmospheric seeing and pointing. Not only does the illumination of the reflector scale as the inverse square of the seeing scale, the finite and small APD field of view truncates flux in poor seeing. Seeing of 2.0 arcseconds produces a return rate ten times smaller than at 1.0 arcseconds, if perfectly centered in both cases. For the present analysis, we use the two highest return rates observed in the first six months of APOLLO operation: 9 December 2005, and 17 January 2006. Both nights had exceptional seeing. On each night, we saw return rates of ≈ 0.5 photons per pulse over < 30 second intervals. In each case, telescope pointing and beam offset were optimized for the best signal.

The estimate of expected lunar rate above is 24 times the observed rate. Even though the analysis is a simplified version, the discrepancy is large, and difficult to eliminate through reasonable choices of parameters.

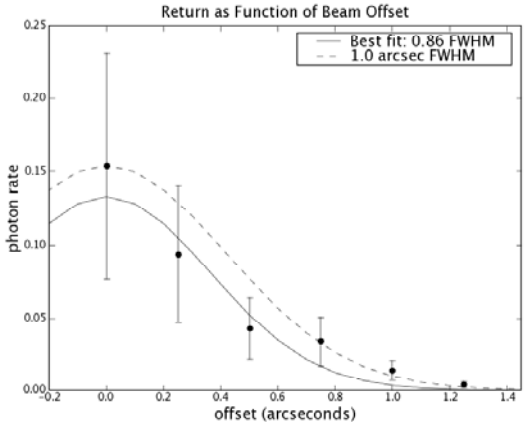

Figure 1*: Beam offset optimization on 9 Dec. 2005. At offset steps of 0.25 arcsec, it is clear that the beam size is less than 1.0 arcsec. Error bars are estimated at 50%.*

The effective beam size on the moon (affected by seeing and optical configuration) is the most obvious place to suspect poor understanding. As for the seeing, the median seeing at the Apache Point Observatory is 1.1 arcsec at zenith. Since the nights used for comparison had especially good seeing, we may assume the seeing to be less than 1.1 arcsec, and likely around 0.8 arcsec. But more convincingly, by rastering the beam pointing on the moon (while keeping the receiver fixed at the same location) we can demonstrate the sensitivity to beam offset, and see directly that the beam illumination footprint on the moon has a full-width at half-maximum (FWHM) less than one arcsecond (Figure 1). Though the best fit in Figure 1 is 0.86 arcsec FWHM, we have chosen 0.8 arcsec in the present analysis because the periods we have chosen for comparison represent the very best 30 second periods within ~10 minute runs. We therefore expect the conditions to have momentarily been better than the average for the run.

It should be noted that the multi-photon capability of APOLLO's detector array renders us insensitive to skewed statistics arising from the structure of the beam's speckle pattern on the moon. In the present analysis, some pulses are seen with as many as 6, 7, or 8 photons. We do not underestimate our return rate by missing these top-heavy events.

Refined Calculation

In the preceding analysis, we made the gross simplifying assumption that the beam patterns were uniform across a circular region—a so-called "tophat" profile. A more realistic calculation should:

- treat the outgoing beam as having a Gaussian profile;
- consider the theoretical diffraction pattern from a perfect corner cube;
- allow for manufacturing tolerance of the corner cubes;
- account for the reduced corner cube throughput as a function of incidence angle;
- de-rate the return strength due to thermal distortions of the corner cube;
- compensate for velocity aberration of the returning beam.

In this section, we treat each of these issues in turn, ultimately producing a more realistic estimate of the return rate, with less uncertainty.

A circularly symmetric Gaussian flux distribution has a peak irradiance that is ln2 ≈ 0.69 times the irradiance of a tophat whose diameter is the same as the Gaussian FWHM and carries the same total flux. Thus we multiply the return rate by this factor.

A corner cube prism employing total internal reflection (TIR) produces a diffraction pattern that is significantly different from that of an equivalent circular aperture. As seen in Figure 2, there is a central core of concentrated flux surrounded by a roughly hexagonal pattern containing significant flux. The core follows the Airy function that would be produced by a perfect circular aperture of the same diameter as the corner cube, but at a peak flux only 27% that of the Airy function, ignoring the two-way reflective surface loss. At normal incidence, the TIR pattern contains 36% of the total energy within the first Airy ring of radius $1.22\lambda/D$, where λ is wavelength and D is the diameter of the aperture [2]. This is compared to 84% for the Airy function.

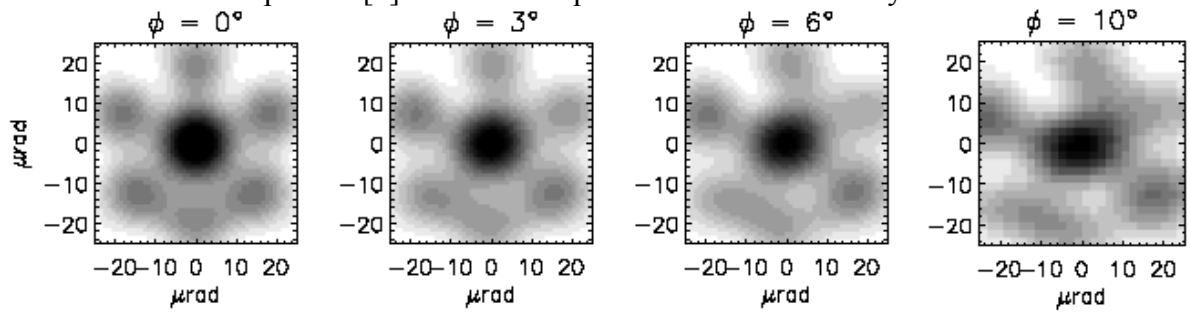

***Figure 2**: Sample diffraction patterns from an Apollo corner cube as a function of incidence angle. Data courtesy David Arnold.*

Compared to a tophat flux distribution with angular diameter λ/D, the normal-incidence TIR diffraction pattern has a central irradiance that is 0.182 times the tophat irradiance if both contain the same total flux. Including the 0.93 two-way front-surface reflection loss from fused silica (η_{refl}), the Apollo corner cubes produce a diffraction pattern with a central irradiance 0.169 times that of the comparison tophat. For the Apollo cubes and $\lambda = 532$ nm, the tophat diameter is 2.89 arcsec.

The manufacturing tolerance for the mutual perpendicular faces of the Apollo corner cubes was specified as ±0.3 arcsec [3]. It was reported that the central intensity of each corner cube selected for flight was at least 90% of the theoretical value. As such, we adopt a factor of 0.93 to provide a representative scaling of manufacturing imperfection.

Corner cubes have an effective cross section that is a function of the incidence angle. For circularly-cut fused silica corner cubes, this function is linear near normal incidence, with 4.3% loss per degree offset. In addition, the Apollo corner cubes are recessed in aluminum mounting structures by half their diameter, or about 1.9 cm. The recesses have conical flares, with half-angles of 1.5° for Apollo 11, and 6° for both Apollo 14 and 15. Together, these factors reduce the throughput by as much as a factor of two for the most extreme libration-induced tilts of 10° (Figure 3).

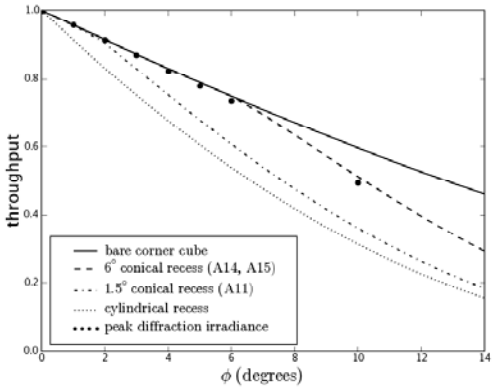

***Figure 3**: Corner cube throughput as a function of incidence angle and recess geometry. The single points come from diffraction patterns (as in Figure 2). Data courtesy Jim Williams.*

The thermal performance of the Apollo reflector arrays in the lunar environment was modeled and tested in great detail prior to flight. The primary performance degradation stems from thermal gradients within the corner cubes, which both deform the optical surfaces and present a refractive index gradient within the material—leading to distortion of the reflected wavefront [4]. For the Apollo 15 array, the central irradiance may be as low as 0.7 times the isothermal value. The original analysis presented plots of degradation as a function of sun angle for the three arrays, from which it is possible to evaluate the thermal degradation factor for any particular lunar phase [5].

Because the lunar reflector is in relative transverse motion with respect to the earth station—due both to the lunar orbit at ≈ 1000 m/s and earth rotation at ≈ 400 m/s—one must account for the angular shift in the diffraction pattern, amounting to $2\Delta v/c$. This amounts to 0.8–1.2 arcsec (4–6 μrad) depending on the vector sum of the relevant velocities. Given the functional form of the central region of the TIR corner cube diffraction pattern, this translates to a signal degradation of 0.64–0.86, or 0.75 on average.

Putting these factors together, we find that the response from the ideal TIR corner cube suffers a factor of 0.20–0.86 degradation. If one then treats the corner cube diffraction pattern as a λ/D tophat function, a pre-factor of 0.034–0.146 must be applied to the link equation. This is equivalent to a tophat function 8–15 arcsec in diameter with no degradation pre-factor.

Analysis of Two Cases

As mentioned before, we use two epochs—both at a return rate of 0.5 photons per pulse—to compare against the return estimate. Table 1 summarizes the various de-rating factors, and estimates resulting from the analysis. The squared atmospheric de-rating as a function of zenith angle has been included (belongs in η_c, technically).

The static factors shown in Table 1 represent the outgoing Gaussian beam profile, the TIR diffraction profile with surface reflection, and the manufacturing tolerance.

***Table 1**: De-rated return rate estimates for the two comparison epochs.*

Parameter	**Epoch 1 value**	**Epoch 1 de-rating**	**Epoch 2 value**	**Epoch 2 de-rating**
Velocity Aber.	1.09 arcsec	0.71	0.86 arcsec	0.81
Angular Offset	3.94°	0.84	4.04°	0.81
Sun Angle	–73°	0.85	35°	0.70
Range	371425 km	1.15	404301 km	0.82
Zenith Angle	50°	0.84	23°	0.97
Static Factors	0.69×0.169×0.93	0.108	0.69×0.169×0.93	0.108
Total de-rating		0.053		0.040
Return Estimate	8.2±3.4 phot./pulse		6.2±2.6 phot./pulse	
Estimate Ratio	16.4		12.4	

Using the de-rating estimates in Table 1 together with Equation (1), and taking the convention that $\Phi = \lambda/D = 2.89$ arcsec, we arrive at the conclusion that we see a return rate approximately 15 times weaker than expected. Given that the estimated net error is about 41%, and considering that this is a multiplicative problem, a one-sigma deviation would correspond to multiplying the estimate by (1 – 0.41) = 0.59. A two-sigma deviation corresponds to multiplying by $0.59^2 \approx 0.35$. To bring the discrepancy down to unity, we must be approximately five standard deviations away—a significant result.

To illustrate the robustness of this result, imagine that our estimate of the beam width—our least certain parameter—is less certain than our ±15% estimate. We could achieve the discrepant ratios by letting the beam profile be as large as 2.8–3.2 arcsec, which is not at all consistent with Figure 1, or APOLLO experience in general.

We conclude that the lunar reflectors have suffered performance degradation (ratios between reflectors are as expected) in their > 35 years on the lunar surface. We cannot tell whether the degradation is due to dust or surface abrasion. Recent work proposing a dynamic fountain of dust on the moon may be relevant [6].

References

[1] Murphy, T. W. et al., "APOLLO Springs to Life: Millimeter Lunar Laser Ranging," *Proceedings of the 15th International Laser Ranging Workshop*, Canberra, (2006)

[2] Chang, R. F., Currie, D. G., Alley, C. O., and Pittman, M. E., "Far-Field Diffraction Pattern for Corner Reflectors with Complex Reflection Coefficients," J. Opt. Soc. America, **61**, 431, (1971)

[3] Kokurin, Y. L., "Laser Ranging to the Moon," *Proceedings of the P. N. Lebedev Physics Institute*, **91**, p. 161

[4] Faller, J. E.., "The Apollo Retroreflector Arrays and a New Multi-lensed Receiver Telescope," *Space Research XII*, Akademie-Verlag, p.235, (1972)

[5] Faller, J. E. et al., "Laser Ranging Retroreflector," Chapter 14 of the NASA post-mission report on the Apollo 15 mission

[6] Stubbs, T. J., Vondrak, R. R., and Farrell, W. M., "A dynamic fountain model for lunar dust," *Advances in Space Research*, **37**, 59, (2005)

Experimental Return Strengths from Optus-B and GPS

John McK. Luck[1] and Chris Moore[1]

1. EOS Space Systems Pty.Ltd., Canberra, Australia

Abstract

The return signal strengths from the retroreflector arrays on the Optus-B satellites in geostationary orbits have been compared with those from GPS targets using the High Energy Laser on the 1.8 metre space debris tracking system adjacent to the Mount Stromlo SLR. In the experiments conducted in mid-2006, we performed alternate ranging to an Optus-B then to a GPS while the two targets were in close proximity to minimize atmospheric differences. Each measurement was the setting of the receive-path Neutral Density filter required to extinguish returns, having first maximized the return rate by fine pointing adjustment.

The ratios of the results, after judicious editing of outliers, were in broad agreement with Dave Arnold's calculations of the respective array cross sections. They suggest that this could be a viable technique for calibrating actual performance of arrays in their space environment.

Satellite Retroreflector Arrays

The constellation OPTUS-B1 and OPTUS-B3 constitutes the space segment of the Australian satellite communications system. They are in geostationary orbits. B1 was launched in 1992 and is at longitude 160°E. B3 (1993) is at 156°E. B2 crashed after launch. Each contains a 20cm x 18cm tray of 14 solid cubes of Herseus fused silica, Amasil grade. Their front faces are tri-roundular with inscribed diameter 38 mm coated with indium tin oxide (ITO) over an anti-reflection dielectric layer. Their rear faces are also coated with ITO and have dihedral angles of 0".8 (James et al, 1990; Luck, 1994). The cross-section of each array is $\sigma_O = 46 \times 10^6$ m^2 (Arnold, 2006).

GPS-35 and GPS-36 each host trays of 32 solid hexagonal cubes 27 mm across with aluminium-coated rear faces. The cross-section of each array is $\sigma_G = 20 \times 10^6$ m^2 (Arnold, 2006). The theoretical ratio of cross-sections is therefore $\kappa = \sigma_G/\sigma_O = 0.43$.

Experimental Method

The method was to range to a pair of satellites, one Optus and 1 GPS, in "bursts" in rapid succession while the selected GPS satellite was "close" to the Optus satellite. During each burst, the Neutral Density (ND) filter was adjusted so that returns were just extinguished. The measurement was the ND value at extinguishment. The UTC, ND setting and GPS elevation angle were recorded at that instant. This method relies on the assumption that the photon detection threshold of the detector is both significant and constant.

"Close" means within a few degrees ($<10^o$) in elevation, to minimize variations in atmospheric attenuation, and also in azimuth to minimize cloud attenuation variation. A "burst" was just long enough to optimize the pointing for maximum return rate, then to adjust the ND until extinguishment, ideally less than 5 minutes. Then a burst was done on the other target.

Observations were made on the 1.8 metre space debris-tracking telescope STRK (7826) adjacent to Stromlo SLR at wavelength 1064 nm, power 2-12 W at 50 Hz.

Data Reduction

Define "brightness" B as the return signal strength (e.g. photons/sec at the detector) when pointing is optimized, and let B_e be the brightness at extinguishment so that it corresponds to the detection threshold. B_e is assumed constant. Let P be the measured average power, effectively equivalent to energy per shot since pulse-width, fire rate etc. are constant. Also let N be the transmission through the ND filter, T be one-way atmospheric transmission, R be the range from station to satellite, and S be the actual array cross-section. Then:

$$B = \alpha P N T^2 . S/R^4$$

where α is a proportionality constant. The observed ratio of cross-sections is then:

$$k = S_G/S_O = (R_G/R_O)^4 . P_O N_O T_O^2 / P_G N_G T_G^2$$

where subscripts G and O refer to GPS and OPTUS respectively. We used $N = 10^{-ND}$ where ND is the Neutral Density wheel setting, and:

$$T = \exp[-0.21072\exp(-h/1.2)/\sin E]$$

where *h* is height above sea level (0.8 Km for Stromlo) and *E* is target elevation angle (Degnan, 1993). The two-way transmission is illustrated in Fig.1.

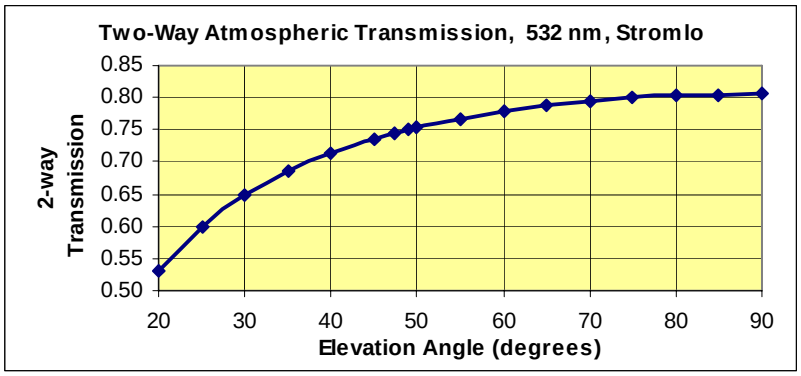

***Figure 1**: Standard atmospheric transmission as a function of elevation angle, Stromlo*

A "standardized brightness" V can be defined for a satellite observed on a given ranging system, as if there was no atmosphere and no ND filter and the transmitted power was 1, normalized to the detection threshold. Thus:

$$V = B_e/PNT^2 \quad \text{and hence} \quad S=R^4V/\alpha.$$

The ratio $\beta = V_G/V_O$ gives the relative standard brightness. Its expected value with R_O = 37180 km (B3, nominal) and RG = 20931 km (GPS36, typical at 49° elevation) is β = 4.28.

Results

Measurements made on 4 clear nights in May 2006 are shown in the Table 1. The column R_G/R_O is the ratio of range (Stromlo to GPS) relative to range (Stromlo to OPTUS). Column S is the cross-sections in square metric (but otherwise arbitrary) units, and column V the standardized brightnesses. There are huge variations, so the greatest and least values of S_G and of S_O were discarded, as were those of V_O and V_G, yielding mean values of:

$S_G = 14.2$ $V_G = 145.8$

$S_O = 34.6.$ $V_O = 34.6$

The ratios of averaged observed cross-sections, and of standardized brightnesses, are:

$S_G/S_O = 0.41$ $V_G/V_O = 4.2.$

The observed cross-section ratio is remarkably close to the predicted $\kappa = 0.43$ given above. The observed brightness ratio similarly is also remarkably close to the predicted $\beta = 4.28$.

Conclusion

It may be that this excellent result is a fluke, but we certainly did not continue observing until we got the right answer! It suggests that this technique might indeed be viable for determining relative cross-sections of retroreflector arrays in actual orbit, provided that a sufficient number of measurements are taken.

***Table 1**: Summary of observations and resulting cross-sections. Optus cross-sections are in green. Rejected outliers are flagged in the right-hand column.*

Date	UTC		Sat	R/R(Opt)	El	P	ND	T	V	S	Rej
May-06	hh	mm			(deg)	(Watts)		(1-way)			
10	9	50	GPS36	0.544	75.9	9	2.75	0.894	78.10	6.84	
	11	2	B1	1	47.4	9	2.15	0.863	21.06	21.06	
	11	9	GPS36	0.598	39.5	9	0.50	0.844	0.49	0.06	*
	11	26	B3	1	48.9	9	4.00	0.866	1480.67	1480.67	*
13	11	0	B3	1	48.9	2	2.00	0.866	66.63	66.63	
	11	10	GPS 36	0.610	40.9	2	3.00	0.848	695.81	96.34	*
	11	20	B3	1	48.9	2	2.00	0.866	66.63	66.63	
15	9	20	B3	1	48.9	12	3.00	0.866	111.05	111.05	
	9	33	GPS36	0.545	85.0	2	1.90	0.897	49.35	4.35	
	9	42	B3	1	48.9	2	0.90	0.866	5.29	5.29	
	9	59	GPS36	0.556	63.6	2	2.30	0.886	127.02	12.14	
	10	3	GPS36	0.560	61.7	2	2.90	0.884	507.80	49.94	
	10	9	B3	1	48.9	2	0.60	0.866	2.65	2.65	
	10	19	GPS36	0.568	55.6	2	2.40	0.877	163.25	16.99	
	10	26	B3	1	48.9	2	0.80	0.866	4.20	4.20	
	10	32	GPS36	0.580	46.2	2	2.10	0.861	84.95	9.61	
	10	42	B3	1	48.9	2	0.80	0.866	4.20	4.20	
	10	44	B3	1	48.9	2	1.00	0.866	6.66	6.66	
	11	0	GPS36	0.603	33.6	2	1.00	0.822	7.39	0.98	
16	9	28	GPS36	0.546	74.8	12	3.50	0.894	329.76	29.31	
	9	44	B3	1	48.9	12	0.60	0.866	0.44	0.44	*
	10	0	GPS36	0.559	62.0	2	1.70	0.885	32.02	3.13	
	10	27	B3	1	48.9	12	2.80	0.866	70.07	70.07	
	10	35	GPS36	0.583	44.4	2	1.20	0.857	10.80	1.25	
	10	42	B3	1	48.9	12	2.30	0.866	22.16	22.16	

Further Suggestions

- Repeat the experiment at 532nm wavelength.
- Extend to GLONASS, GIOVE, ETS-VIII, LARES and others.
- The GPS array is theoretically about 1500 times brighter than Apollo 15, corresponding to ND 3.2, so if GPS is still observable at a station with this setting then LLR should also be acquirable.

- Systems having readouts for return signal strength would be well suited to doing an equivalent of this experiment, more easily. In fact, by using our method as well as their own, our method could be tested.
- Similarly, comparisons of return rates in controlled experiments might assist in validation of the technique.

References

[1] Arnold, D.: Private communications, 2006.

[2] Degnan, J.J.: "*Millimetre Accuracy Satellite Laser Ranging: A Review*", in "Contributions of Space Geodesy to Geodynamics: Technology", David E. Smith & Daniel L. Turcotte (Eds), Geodynamics Series Vol.25, American Geophysical Union, Washington D.C., esp. pp.139-140 (1993)

[3] James, W.E., W.H. Steel & Evans, N.O.J.L: "*Design and Testing of a Cube-Corner Array for Laser Ranging*", SPIE Vol.1400 Optical Fabrication and Testing, p.129 (1990)

[4] Luck, J.McK. & J.R. Woodger: "*Laser Ranging Support for TV Time Transfer Using Geostationary Satellites*", Proc. 8th European Frequency and Time Forum, Technical University Munich, March 9-11, 1994.

Spherical Glass Target Microsatellite

V.D. Shargorodsky, V.P. Vasiliev, M.S. Belov, I.S. Gashkin, N.N. Parkhomenko

1. Institute for Precision Instrument Engineering, Moscow, Russia.

Contact: www.niipp-moskva.ru

Abstract

A new SLR target microsatellite based on the optical Luneberg lens concept is now undergoing ground testing. It will be launched from the carrier spacecraft METEOR-M next year, and will be the first autonomous retroreflector satellite of this type, providing an extremely low target error.

Some parameters are presented of the microsatellite and its orbit, as well as far-field diffraction patterns measured on test bench.

Introduction

Most of the current SLR target satellites are spherical structures carrying a number of corner cube retroreflectors; with the rapid progress in SLR precision during the last decades, some disadvantages of such targets, being insignificant during the first years of SLR development, became increasingly more significant with the passing years.

The disadvantages are:

- It is difficult to obtain target errors less than 1 mm if return signals come from several cube corners having different positions relative to the CoM (Center of Mass) of the satellite.
- Even if the "one direction - one reflector" principle is used (e.g. in the WESTPAC or LARETS satellite design), the active retroreflector position varies relatively to the CoM, and the cube corner internal delay time also varies when the active retroreflector moves away from the line connecting the SLR system with the satellite CoM.
- The return signal strength varies significantly with the satellite rotation.
- The satellite shape is not an ideal sphere, especially for a design using the "one direction - one reflector" principle (WESTPAC, LARETS).
- Interaction with the Earth magnetic field (due to eddy currents induced in the massive metal body): slow-down of spinning, some disturbance of orbital motion.

There is a way to overcome the above difficulties. Instead of a multitude of corner cube prisms mounted on a spherical metal body, the target may be a single spherical retroreflector made of glass.

The initial idea was to use a device similar to the Luneberg lens proposed in 1944 and used in some radio-frequency systems (Figure 1). A planar electromagnetic wave coming from any direction is there focused on opposite surface of the spherical lens and if this surface is a reflective one, the device acts as a retroreflector.

Unfortunately, there are currently no suitable optical materials for correct implementation of such a device operating in the optical waveband.

A possible solution is using of a ball lens made of a glass with an index of refraction exactly equal to 2 (Figure 2). However, it requires a special extra-dense glass of a

high optical quality; this is currently a very hard task. Moreover, calculations show that only a small part of the ball aperture may be effectively used because of the spherical aberration.

The first practical solution was a two-layer glass ball, where the inner part is made of a flint glass having a relatively large index of refraction (1.75), while the outer layer is made of a crown glass with a low index of refraction (1.47). Such a device has been implemented and successfully tested showing acceptable retroreflector parameters [1] (Figure 3).

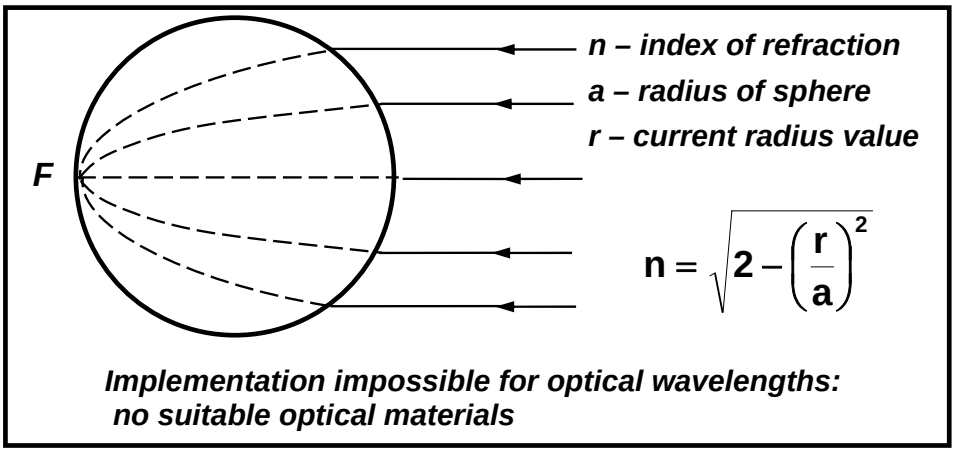

Figure 1. *Luneberg lens principle*

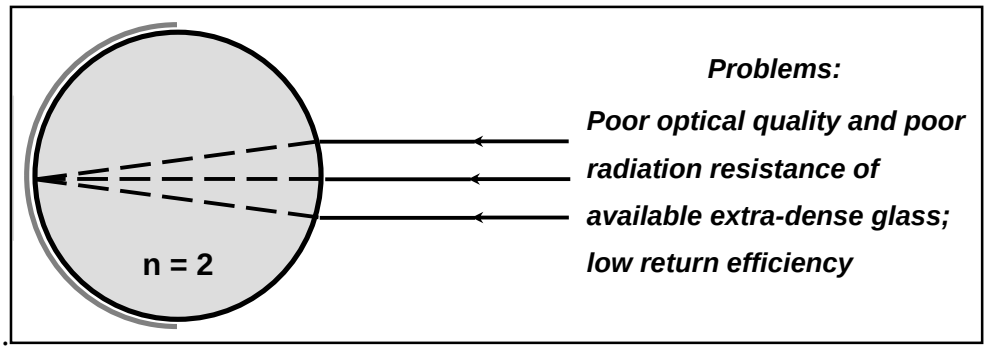

Figure 2. *Ball lens made of glass with index of refraction n = 2*

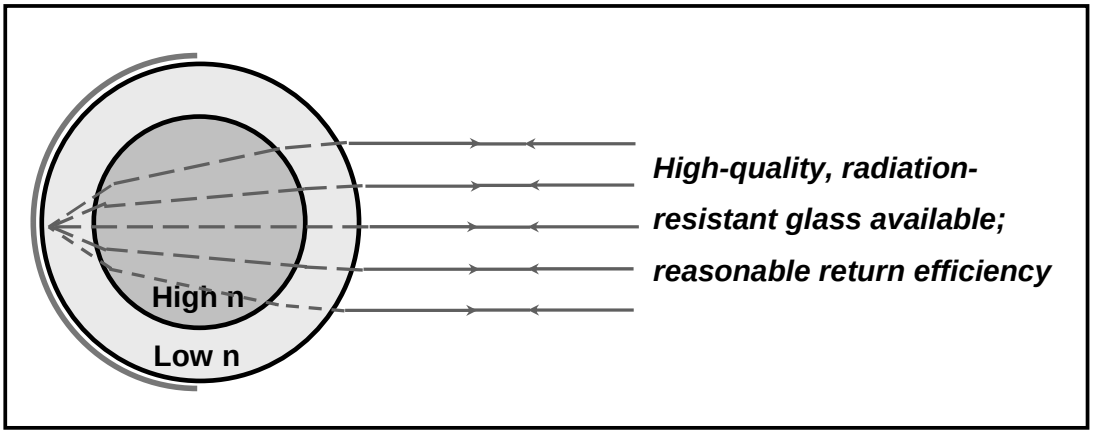

Figure 3*. Spherical retroreflector: a two-layer ball lens*

An experimental 60-mm-diameter spherical retroreflector of this type [2], after being tested in laboratory conditions, has been 10 December 2001 launched into space on board of the METEOR-3M(1) satellite having a 1018.5-km-high circular orbit (Figure 4). During four years of operation, the spherical retroreflector provided precision orbit determination for the SAGE-III experiment.

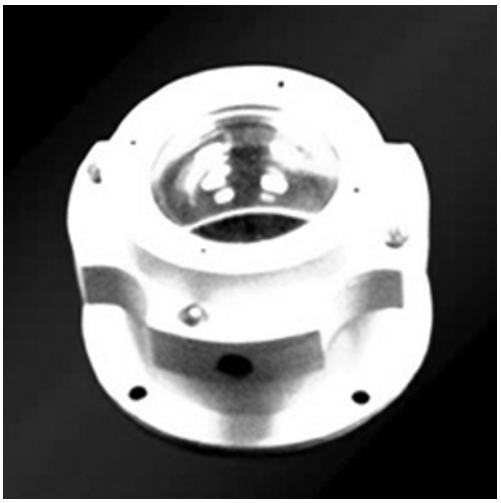

Figure 4*. An experimental 60-mm-diameter spherical retroreflector, launched into space on board of the METEOR-3M(1) 10 December 2001*

The lidar cross-section of this target was low (about 10^4 sq.m at the initial phase of flight), making SLR observations difficult and even impossible for a large part of the ILRS network stations.

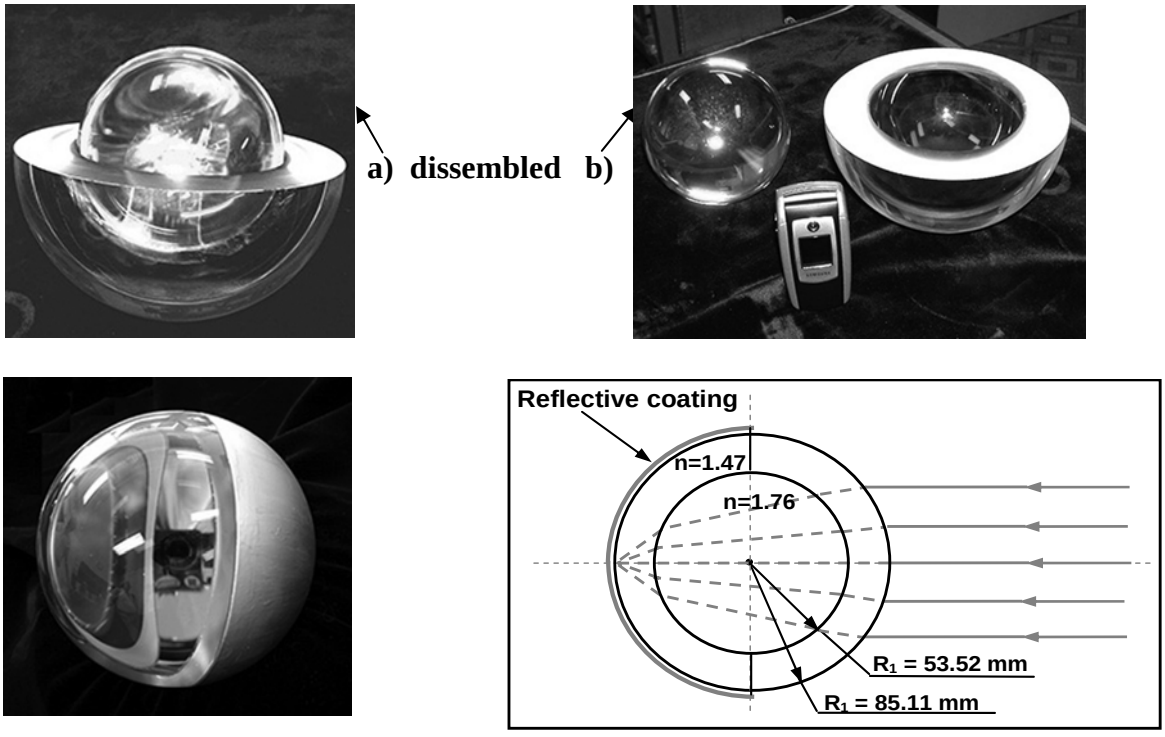

Figure 5. *17-cm-diameter spherical retroreflector*

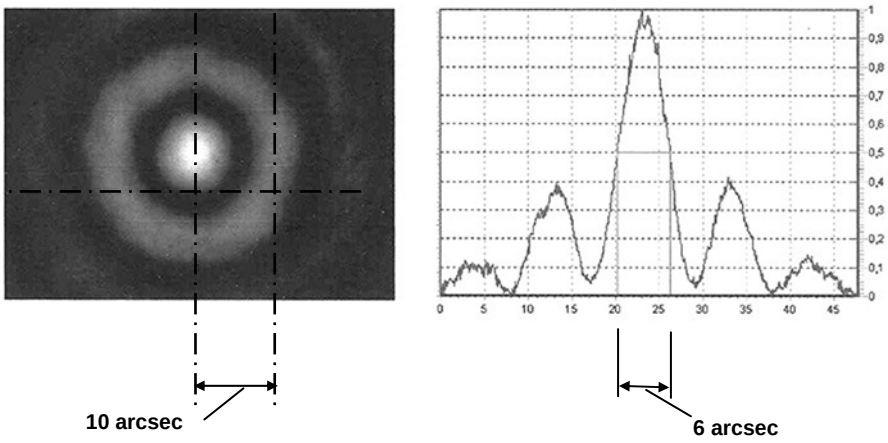

Figure 6. *Far-field diffraction pattern*

We have therefore developed and fabricated a medium-size (17 cm in diameter) spherical retroreflector of this type, which can be used as an autonomous SLR target.

Figure 6 shows the far-field diffraction pattern of this device measured on a test bench. It can be seen from the picture, that most of the return signal energy is in the first-order side lobe (the product of its amplitude and solid angle is more than that of the center lobe).

It is intended to launch this device as an autonomous SLR target, as a piggyback load on the Meteor-M spacecraft. The basic parameters of this micro-satellite are shown in Table 1.

Table 1. *Zero-signature spherical retroreflector micro-satellite*

Microsatellite parameters	
Diameter	17 cm
Mass	7.45 kg
Cross-section	~100,000 sq.m at λ=532 nm
Current status	
Return pattern measurement under varying ambient conditions	
Separation system development	
Mission	
Carrier satellite	METEOR-M
Carrier satellite parameter	Height: 835 km (circular) Inclination: 99.7°
Planned launch date	Late 2007

The separation system (now under development) should provide a spin rate of at least 6 rpm, while the spin axis lies in the plane dividing the ball lens surface into the coated and uncoated parts.

SLR targets of this type may be improved in the following ways:

1. To increase the lidar cross-section, more than two layers of glass may be used. Calculations show that a three-layer ball lens may provide a significantly higher cross-section value than a two-layer one.

2. To provide operation on two widely separated wavelengths (e.g., 532 nm and 1064 nm), a design may be used shown in Figure 7. In the future, such an SLR-target may be attractive for minimization of the atmosphere refraction error using simultaneous two-wavelength ranging.

3. If (or rather when) super-dense optical glass with reflection index values ≥2 with good optical quality becomes available, it may be used for manufacturing of a ball-lens retroreflector microsatellite with a high mass to aperture cross-section ratio.

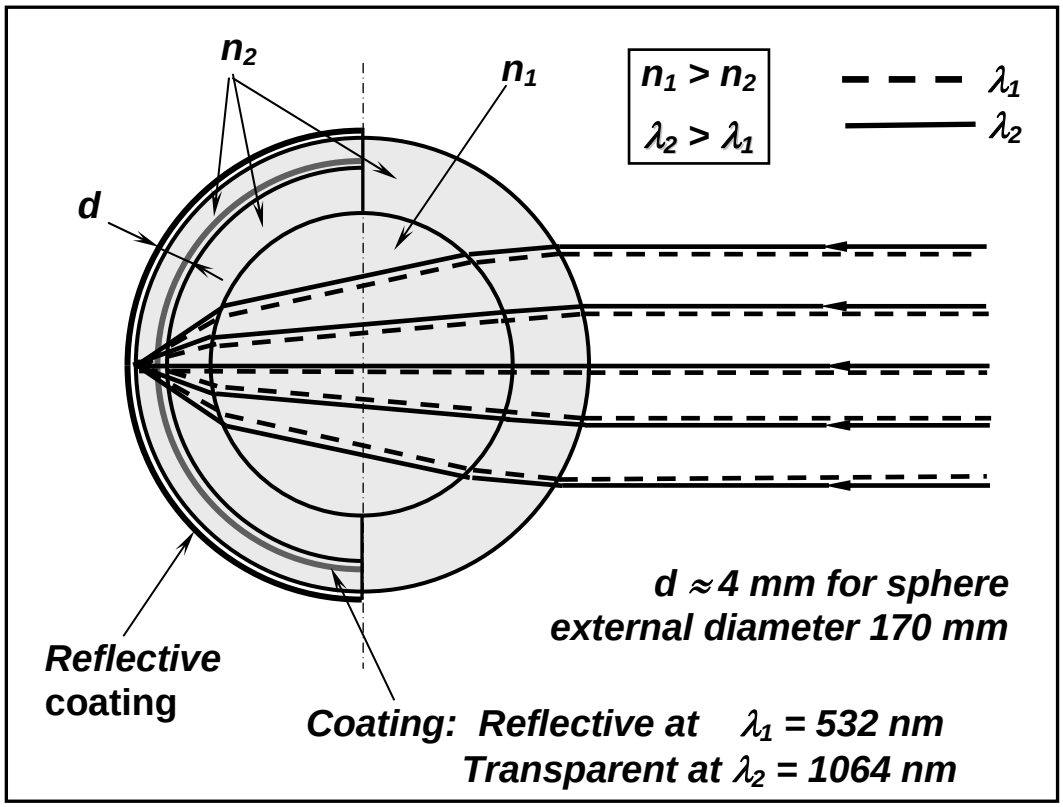

Figure 7. *Spherical retroreflector for operation at two widely separated wavelengths*

References

[1] Vasiliev V. P., Gashkin I. S., Belov M. S., Shargorodsky V. D., A New Approach to a Submillimeter SLR Target Design. Proceedings of 11th International Workshop on Laser Ranging, Deggendorf, Germany, Sep. 1998

[2] Shargorodsky V. D., Vasiliev V. P., Soyuzova N. M., Burmistrov V.B., Gashkin I. S., Belov M. S., Khorosheva T. I., Nikolaev E. A. Experimental Spherical Retroreflector on Board of the Meteor-3M Satellite. Proceedings of 12th International Workshop on Laser Ranging, Matera, Italy, 2000